SUPPORTING INFORMATION

1 Materials

The results and discussion sections of the main manuscript and Tables 3 and 4 in the main manuscript present and discuss physical-chemical properties in detail. The following sections provide additional information on the production process of ENMs and NEPs, their visual appearance and micromorphology.

1.1 Benchmark Materials

Benchmark materials were selected from the JRC repository of the OECD sponsorship program for the testing of nanomaterials except for Mn_2O_3 (Skyspring nanomaterials, Houston, USA) and CuO (PlasmaChem, Berlin). Both material were from fresh batches of the same grades previously tested in the SUN project.(Pantano et al. 2018; Hristozov et al. 2018; De Jong et al. 2018; Gosens et al. 2016)

ZnO nanomaterials (NM110 and NM111 from the JRC repository) were re-characterized to optimize the comparability within our dataset, despite earlier data from JRC reports.(Singh et al. 2011) Multi-wall Carbon Nanotubes (mwCNT) were obtained in two NFs, NM400 and NM402, from the JRC repository, and were re-characterized despite earlier existing data from JRC reports.(Rasmussen et al. 2014)

1.2 Case Studies: Powders and Suspensions (ENM)

The case study materials cover a wide range of the materials that are prioritized by the French R-nano reporting with high tonnages, and include some novel materials.

Wet phase synthesis with precipitation in water or solvents, then drying to the commercialized powder, is used to produce the DPP, Fe_2O_3 and CuPhthalocyanine pigments (all from BASF Colors and Effects), as published previously. The batches are identical to previous studies on individual aspects of the safety assessment.(Pizzol et al. 2019; Amorim et al. 2018; Neubauer et al. 2017; Pang et al. 2017; Arts et al. 2016)

The cementitious materials were successively micronized and nanostructured (all at Zoz GmbH, Wenden, Germany) to increase reactivity in the cement hydration, starting from granulated blastfurnace slag (GBS), to then obtain ground granulated blastfurnace slag (GGBS), then high-energy milled in order to create activated nanostructures (HKP_GGBS_hr). Portland cement (CEM), of grade CEM I 52.5R, was obtained from, HeidelbergCement AG, Heidelberg, Germany.(Funk et al. 2019) The nanostructured additives GGBS and HKP_GGBS_hr (High Kinetic Processing-GGBS, highly reactive) were obtained by processing of a commercial granulated blastfurnace slag (GBS, ThyssenKrupp Steel Europe AG, Duisburg, Germany). For comminution in the first step to obtain GGBS, 5 kg of GBS were dried at 60°C and milled (drum mill Comb03-A03, Zoz GmbH, Wenden, Germany) with 44 kg corundum balls (ball diameter between 5/4” and 7/8”, total filling level of 66.7 vol.-%) at 50 rpm for 4 h. In a second step, GGBS was further comminuted, nanostructured and activated to HKP_GGBS_hr by high kinetic processing (Simoloyer® CM08-8lm, Zoz GmbH, Wenden, Germany).

Wet phase synthesis by Stoeber processes generates the colloidal SiO_2 materials, which are commercialized as aqueous suspension. The materials tested here were the same grade but reproductions by different batches of the same sizes and surface modifications as in earlier studies.(Arts et al. 2016; Wohlleben et al. 2016; Landsiedel et al. 2014) We included a pyrogenic (NM203) powder from the JRC repository, which have been extensively characterized previously.(Farcal et al. 2015; Schneider et al. 2011)

The CeO_2 NM211 and NM212 materials were produced by precipitation, and were obtained from the JRC repository. Many physical-chemical parameters were published in from earlier studies.(Keller et al. 2014) The nanoforms of TiO_2 NM102, NM104, NM105 were obtained from JRC repository, and

were complemented by a surface-coated non-nano-form of TiO_2 (pigment white, for paints and coatings) from Kronos; its production process has not been disclosed.

Nominally monolayer graphene and multilayer graphene (ACS nanomaterials) were produced by undisclosed processes. Carbon Black (Ensaco) is produced by pyrolysis and was a grade optimized for conductive quality, not for rubber/tire applications. WS_2 forms are stiff inorganic nanotube-like fibres (length 1 to 20 µm) generated from Tungsten oxide and H_2S or sulfur by high-temperature sulfidation (Apnano, Israel). In contrast to CNTs, the production process does not involve toxic catalyst substances possibly influencing biological properties.(Visic, Panchakarla, and Tenne 2017; Zohar et al. 2011)

In contrast to the other materials, Kaolin is a naturally occurring nanomaterial of platelet shape, differing in thickness and lateral dimensions. Kaolin is mined and commercialized after purification (BASF SE) for paper, paint and polymer reinforcement applications. The IRMM385_Kaolin was assessed before by the NanoDefine project, and was provided by JRC Geel, Belgium.(Babick et al. 2016)

$BaSO_4$ is produced by precipitation, grinding and washing. The NM220 was provided by the JRC repository Ispra, and was extensively characterized before. The IRMM381 non-nano-form was assessed before by the NanoDefine project, and was provided by JRC Geel, Belgium.(Babick et al. 2016)

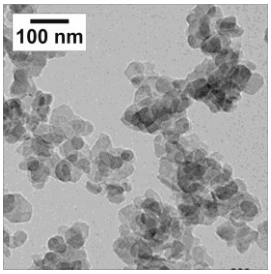

DPP_nano

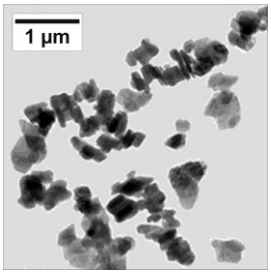

DPP_non-nano

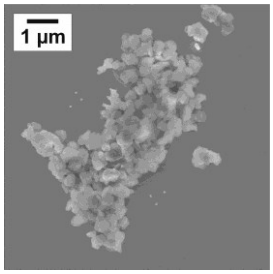

DPP_coated

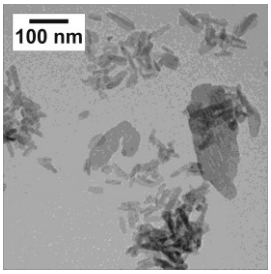

CuPhthalo_nano

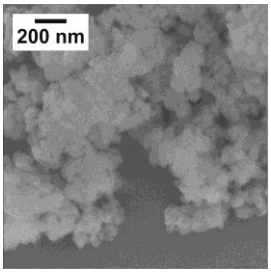

CuPhthalo_halogen

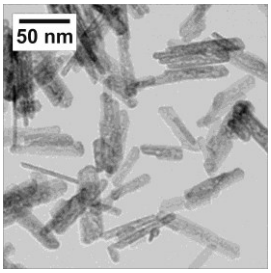

Fe2O3_nano_A

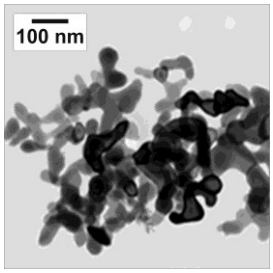

Fe2O3_nano_B

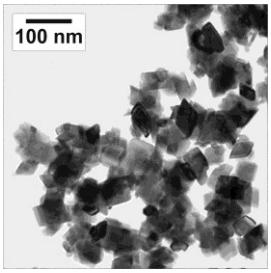

Fe2O3_larger

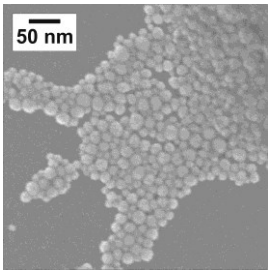

SiO2_untreated

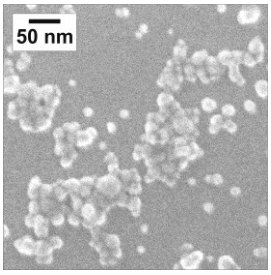

SiO2_amino

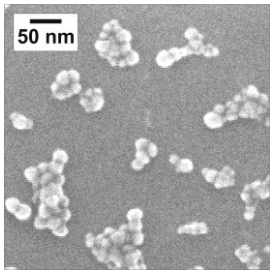

SiO2_phosphonate

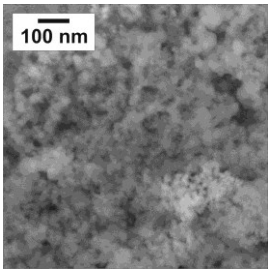

NM203_SiO2_hydrophil

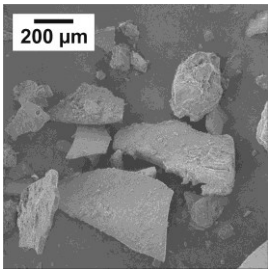 GBS	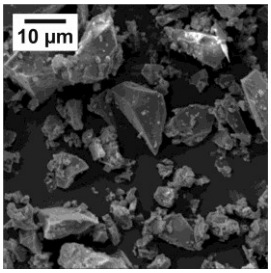 GGBS	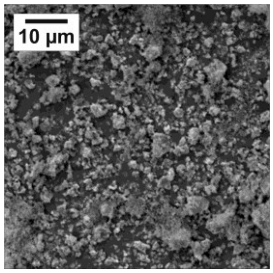 HKP_GGBS_hr	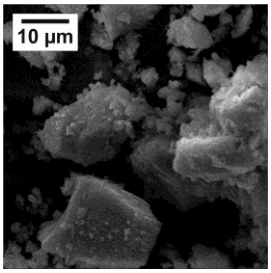 CEM
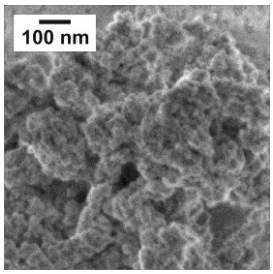 NM211_CeO2	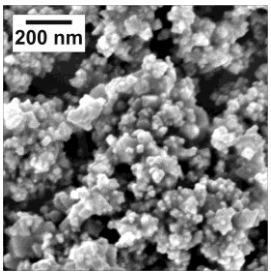 NM212_CeO2	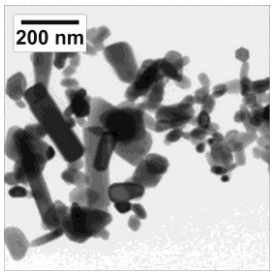 NM110_ZnO	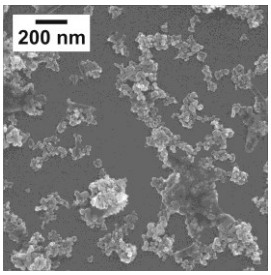 CuO
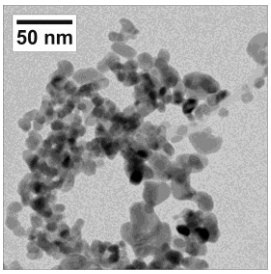 NM105_TiO2_nano	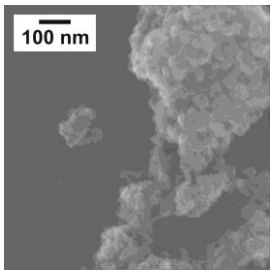 NM102_TiO2_nano_activ	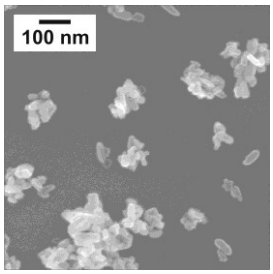 NM104_TiO2_nano_coated	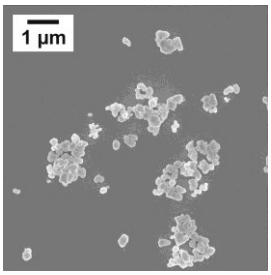 TiO2_non-nano
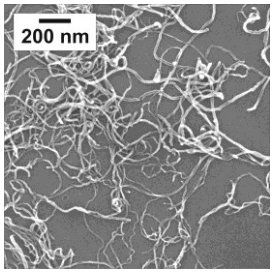 NM400_CNT	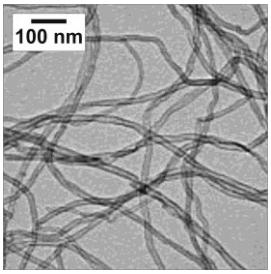 CNT_in_Composite (grade NC7000)	Carbon Black	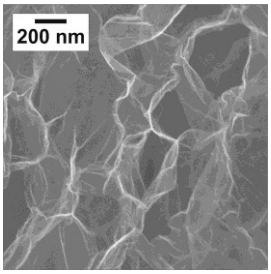 Graphen_monolayer
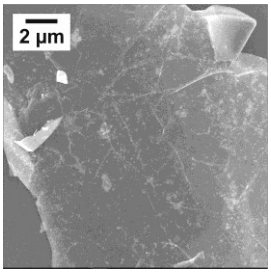 Graphen_multilayer	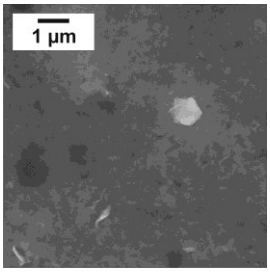 NM600_Bentonit	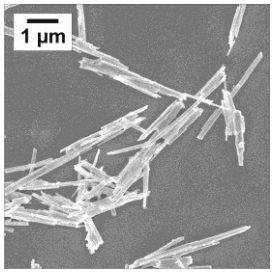 WS2	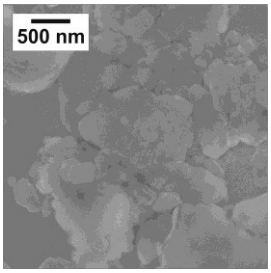 Kaolin

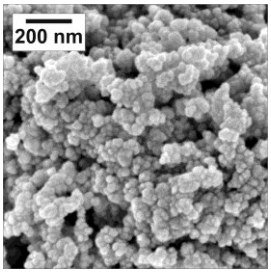

NM220_BaSO4

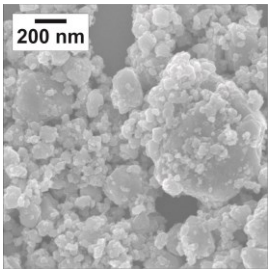

Mn2O3

Figure SI_1 Representative electron microscopy (SEM or TEM as appropriate) of the pristine NM (Tier 1)

1.3 Case Studies: Nano-Enabled Products (NEP)

The cement pastes were prepared with technically relevant amounts of additives and a constant water to cement ratio (w/c) of 0.4 according to DIN 1045-2:2008 to ensure complete hydration and hardening and to prevent incomplete binding. For the preparation of the nanomaterial-containing cements pastes (CEM with SiO2, or TiO2), the nanomaterials were dispersed homogenously in the mixing water with the addition of a superplasticizer (MasterGlenium® SKY 592, BASF Construction Solutions GmbH, Trostberg, Germany) prior the addition of cement. In the case of the blast furnace slag composites (CEM with GGBS or HKP_GGBS_hr), the slag and the cement were dry mixed in advance by a continuous ploughshare mixer. The components of each composite were then stirred with mixing water at room temperature for at least 2 min, and were casted in 100x100x100 mm³ cubes (Figure SI_2_a to d)) according to EN 12390-2:2009, and were stored according to DIN EN 196-1:2016 for at least 28 days under wet conditions at room temperature.

The automotive coating NEPs were prepared by dispersing at 3% by weight three nanosize pigments (DPP_nano, Fe_2O_3 and CuPhthalo_nano) in a mixture of acrylic and polyester polymers. The pigments were stirred in a standard solvent-borne coating with a disperser. The coating was applied on a steel test panel by spray application and hardened in an oven. The resulting plates measured 10 cm x 9 cm.

Different NEP nanocomposite plates (5 cm x 5 cm) that perform well for lightweight mobility applications were generated using epoxy and thermoplastic (PA and PP) polymers. Epoxy plates were mixed and cured with MWCNT (Nanocyl 7000, 0.38% (w/w) = 0.22% (v/v)), WS_2 nanotubes (ApNano, 1.5% (w/w) = 0.22% (v/v)), multilayer graphene (ACS, 1% (w/w) = 0.6% (v/v)), carbon black (Ensaco conductive grade, 3.4% (w/w) = 2% (v/v)), and SiO_2 (Aerosil, 3% (w/w) = 1.5% (v/v)). For the 2D and 1D materials respectively, a lower concentration was chosen to represent the real-world benefit of lower-dimensionality material that achieve percolation and thus conductivity at reduced filler content.(Neubauer, Wohlleben, and Tomović 2017). The thermoplastic nanocomposites were prepared by combining PA with Kaolin (25% w/w) and PP with CuPhthalo_nano (0.5% w/w) employing hot melt extrusion process.

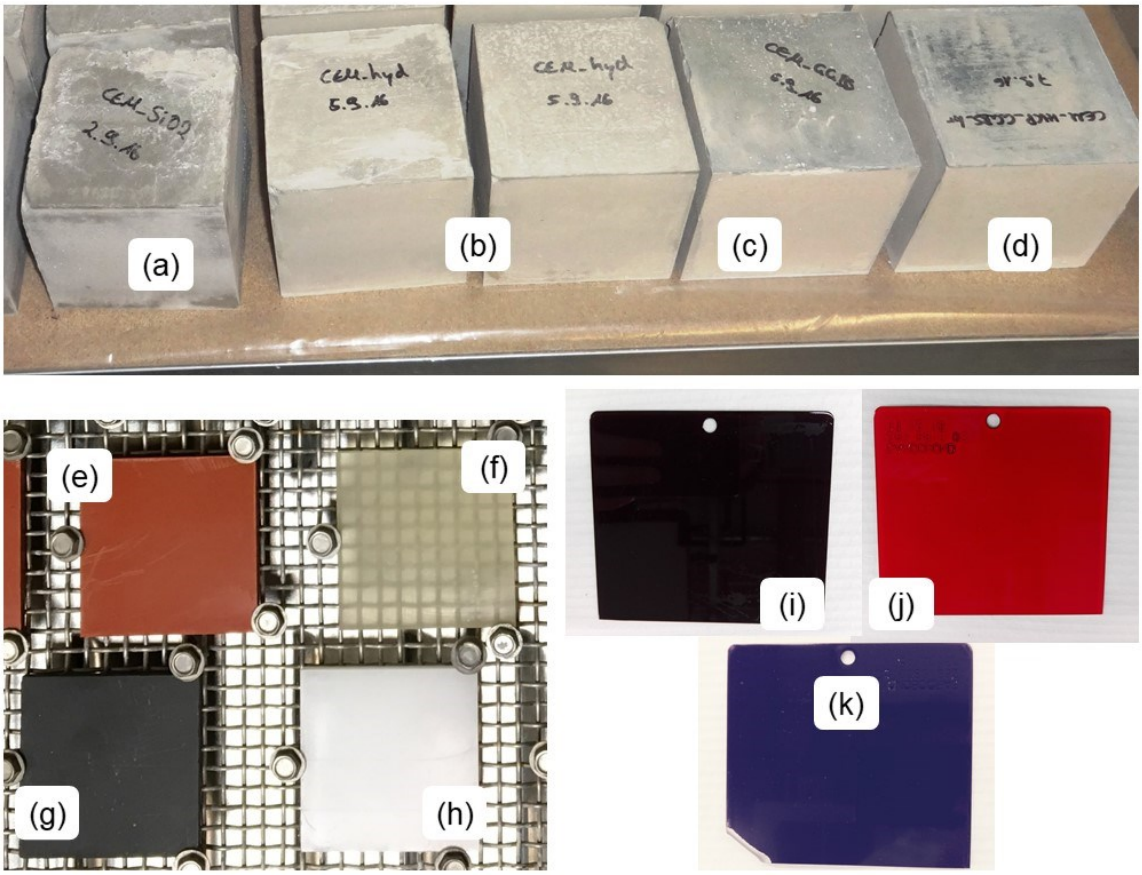

Figure SI_2 Illustrative photographs of the test specimen of nano-enabled product (NEP): (a-d) cement/concrete cube (10 cm edge length), (e-h) polymer (5 cm edge length) and (i-k) coating plates (9 cm edge length).

(a-d) High purity Portland hydrate cement/concrete composites with (a) silica NPs (SiO_2), (b) no filler, (c) ground granulated blast furnace slag (GGBS) and (c) high kinetic processing-GGBS (HKP-GGBS). (e-h) Selection of polymer plates: (e) polypropylene filled with Fe_2O_3, (f) unfilled epoxy, (g) epoxy embedded with carbonaceous NPs and (h) unfilled polypropylene. (i-k) Three acrylic coating plates embedded with (i) Fe_2O_3, (j) DPP_nano and (k) Cu-Phthalo_nano.

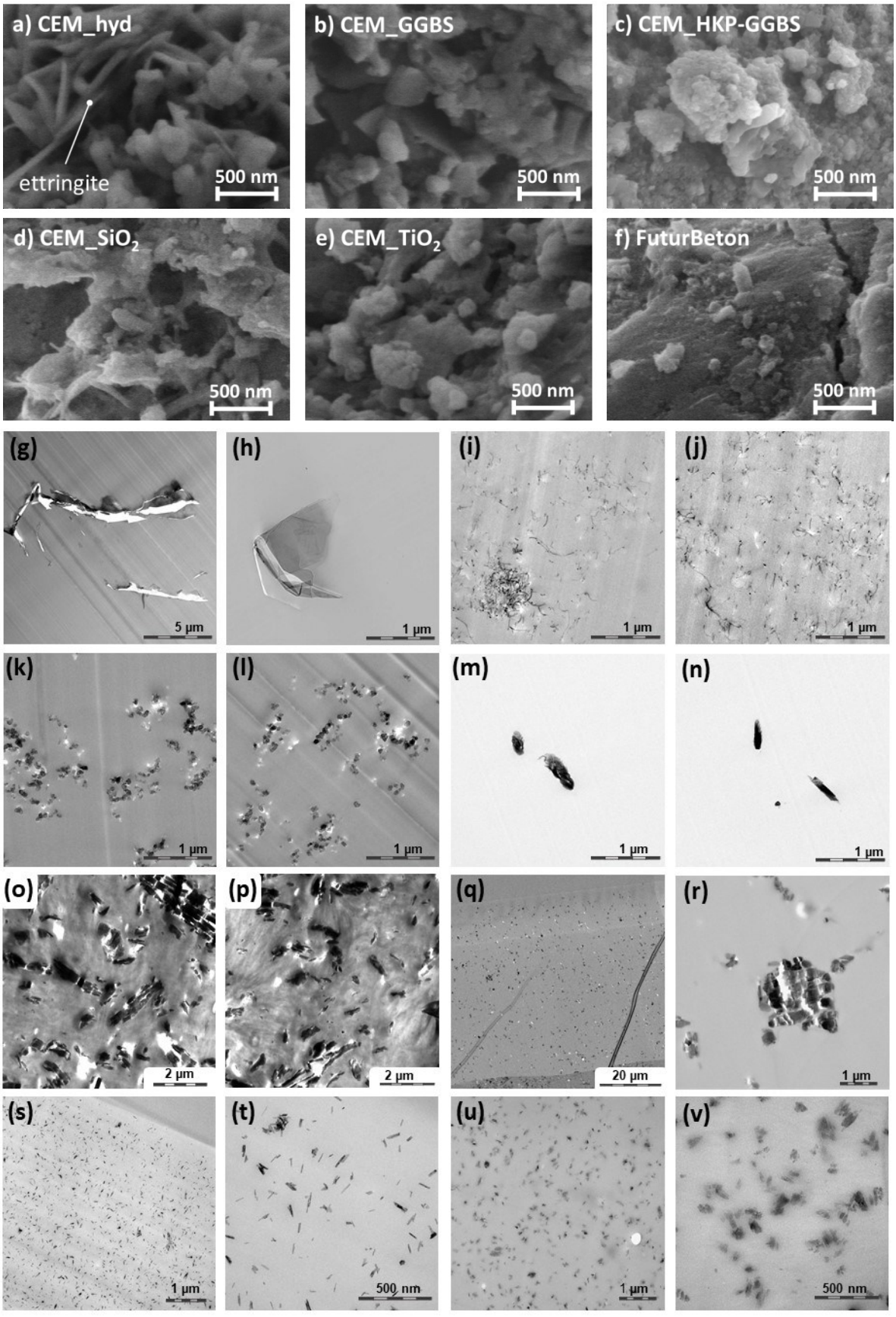

Figure SI_3 Representative electron microscopy characterization of (a-f) cement/concrete specimens, (g-p) polymer and (q-v) coating plates.

(a-f) SEM analysis of high purity Portland hydrate cement/concrete composites with (a) no-filler (CEM_hyd) and with 5 other different additives: (b) ground granulated blastfurnace slag (GGBS), (c) high kinetic processing-GGBS (HKP-GGBS), (d) silica NPs (SiO_2), (e) titania NPs (TiO_2) and (f) mix of HKP-GGBS, sand and coarse grain (FuturBeton).

(g-v) Cross-sectional TEM evaluation of different plates: (g-n) epoxy plates embedded with (g, h) graphene, (i, j) carbon nanotubes, (k, l) carbon black, (m, n) tungsten disulphide; (o, p) polyamide plates filled with high content of Kaolin; (q-v) acrylic coating incorporating (q, r)) DPP, (s, t) Fe_2O_3 and (u v) Cu-Phthalo nano-pigments.

2 Methods

2.1 Properties, which describe the „what they are: physical structure“

2.1.1 Primary particle geometry and primary particle dimensions

Both properties are recommended by ECHA best practice as an essential description of a nanoform. If a material has been identified as a nanomaterial with the NanoDefine methodology, electron microscopy may already be present. The nanoGRAVUR-relevant descriptors of the "minimum external dimension" and the "aspect ratio" can then be read directly from the pdf report of the NanoDefiner-etool. Otherwise, SEM or TEM must be measured. Image analysis should use the NanoDefiner e-tools, as documented in the "NanoDefine Methods Manual" (http://www.nanodefine.eu/index.php/nanodefine-publications/nanodefine-technical-reports).

2.1.2 Rigidity (esp. for fibers)

We suspect that rigidity is a crucial property for grouping of fibers, possibly even for classification (by carcinogenicity). So far no method for the experimental determination of the rigidity for the regulatory or industrial routine operation is foreseeable. Table 3 in the main manuscript therefore uses a diameter value as a replacement criterion, an interim value for potentially critical rigidity for multiwall CNT. In the current nanoGRAVUR scheme, rigidity is not determined experimentally and is not used quantitatively.

2.2 Properties which describe the „what they are: chemical composition“

2.2.1 GHS CLP human toxicity (bulk material)

The GHS codes (globally harmonized system) of the same composition in a non-nano-form ("bulk"), as established in the CLP (classification and labelling of products) directive can be taken as a first indication of a potential hazard from nanomaterials of the same substance. Both physical and health hazards (Chapter 2 and Chapter 3, CLP) are considered. It is assumed that the nanomaterial has the same or more GHS codes than the bulk material. Both the harmonized and the self-ratings are considered, as published on the ECHA website (https://echa.europa.eu/information-on-chemicals). Level 1 Harmonized Classifications (e.g., Pyr Sol 1, Carc 1B) are considered critical. Self-rated class 1 or higher classifications are considered as an indication of a hazard. This information is useful for targeted but does not serve the comparison between two NFs, as the property is always the same for both NFs. The GHS codes are especially important for grouping by consumer safety, which however was not formalized to the same extent as the grouping by environmental safety and by occupational safety.

2.2.2 GHS CLP ecotoxicity (reference material, bulk)

This parameter is used to integrate the material toxicity in the assessment. For (nearly) insoluble nanomaterials, it uses information for the bulk materials with a particle size >1 µm. For nanomaterials whose toxicity is significantly caused by released ions, the orientation factor is the toxicity of a soluble

salt. Toxicity is represented by the EC50. In the worst case scenario, toxic substances whose toxicity falls below the value that characterizes the ecotoxicity classes with the lowest ecotoxicity listed in various regulations (100 mg/L, 1000 mg/kg) are considered toxic. This information is useful for targeted but does not serve the comparison between two NFs, as the property is always the same for both NFs. More details are discussed elsewhere.(Hund-Rinke et al. 2018)(Kühnel et al, 209, submitted)

2.2.3 Solubility in water

The OECD TG "*OECD test guideline for the testing of dissolution rate of nanomaterials in aquatic media*", currently being drafted, describes a "screening dissolution test", ideally suited to recognize easily soluble substances. It describes a minimum of two test concentrations, three pH values in 5 mM bicarbonate buffer, and a separation of undissolved matter from ions by ultrafiltration or ultracentrifugation after 24h. We follow the same logic but simplify requirements for the purpose of comparing between NFs.

The data shown in Table 3 was acquired with initial ENM concentrations of 100 mg/L in pure water and 1000 mg/L in ecological media, but for future studies nanoGRAVUR recommends to adhere to the draft OECD guidance, specifically ultrafiltration over 5 kDa membranes for separating the ions from the remaining particles, and screening only in H_2O at pH 7, only at 10 mg/L, to remain consistent at the same time as increasing efficiency.

Since the ion concentration is measured in equilibrium, it is possible that poorly soluble materials are not recognized as being soluble but will prove biosoluble outside of equilibrium (in environmental compartments or in a physiological environment). The benchmark material is described in the draft TG as "Copper(II)oxide (<50 nm, SA: 29 m^2/g, non-coated) available through the JRC", and is sufficiently similar to the CuO in nanoGRAVUR.

2.2.4 Physico-chemical hazards (bulk)

The globally harmonized system (GHS) is used. No specific requirements. This information is useful for targeted testing by specific scenarios in tier 3, but is irrelevant for the Tier 2 comparison between two NFs, as the property is always the same for both NFs.

2.3 Properties, which describe „what is the NEP"

2.3.1 Product classes and application scenarios

For the purpose of downstream professional user or consumer protection, the following four product classes are distinguished: powder, suspension, spray and solid. With regard to the application scenarios, the different routes of exposure are considered, and for consumer protection are weighted with regard to the main route(s) of exposure (application) and also including further routes (misuse or accident).

2.3.2 Specific NEP: Dispersion state of the ENM

This property describes whether the primary particles are bound to each other or in a continuous matrix (liquid or solid). The criteria listed relate to a specific application subdivided into the product classes (see 2.3.1). If the framework is applied to nanomaterials before integration in NEPs, one should assess whether the particles or fibers are present as sintered aggregates, which cannot be broken up with realistically expected forces. The quality of the SEM or TEM scan is used to evaluate

whether sintered necks are recognizable. This is the case for fumed silica (NM203), but not for colloidal silica (SiO2_untreated)

As a future quantitative method, it would be conceivable to carry out either wet dispersion with a certain ultrasound energy density (and "optimal additives" for stabilization until measurement), or dry dispersion in the aerosol, but data for deriving band boundaries are not sufficiently available. (Retamal, Babick, and Stintz 2017; Göhler and Stintz 2015).

2.3.3 Specific application in the NEP: Content of the ENM

The gravimetric content should be known from the composition of the NEP, or must be determined, mostly via element-selective methods (e.g. ICP-OES, XRF). If nothing is known about the NEP, grouping is probably not the most direct route to risk assessment, even though some of the same characteristics may be relevant, but then in other assessment schemes (Oomen et al. 2018).

2.4 Properties, which describe „where they go: release / exposure“

2.4.1 Dustiness

Dustiness or dustiness of a material is a test method specific characteristic for describing the dust evolution behavior of powders in typical handling processes (e.g., falling, mixing, dumping). It is typically expressed in terms of mass-specific dust fractions [mg/kg, #/kg].

Today, there are numerous national and international standards that deal with methods for determining dustiness (eg: EN 15051-2: 2013, EN 15051-3: 2013, DIN 55992-1, DIN 55992-2, VDI 2263-9, DIN 33897-3, BGI 5047). An overview of the classical methods can be found in (Hamelmann and Schmidt 2003). Most widely used are the method for the continuous fall in the counterflow (CCD: Continuous drop down) and the repeated case within a rotating drum (RD: rotating drum). Since classical methods such as CDD, RD sometimes require significant amounts of test material, numerous new methods have been developed in the last 15 years (see also ISO / TS 12025: 2015) which are gaining increasing international recognition. These are essentially the Small Rotating Drum (Schneider and Jensen 2008) as well as shaking and fluidized bed methods (Ogura, Sakurai, and Gamo 2009; Plitzko et al. 2010). At present, the comparability of the methods has not yet been conclusively clarified. Therefore, for example, a grouping based on data determined using a consistent methodology should not be substantiated with mixed methods.

From the point of view of nanoGRAVUR both the use of the EN 15051 methods (CDD, RD) as well as of alternative methods (SRD (small rotating drum), FLU (fluidized bed), DEM (dustiness equivalent method based single drop down)) with comparable low dry dispersion intensity are recommended. To assess the dusting tendency, method-specific property boundaries are to be used which are to be determined by means of suitable benchmark materials (for example $BaSO_4$, NM203_SiO2, NM400). For CDD and RD band boundaries are specified in EN 15051-2: 2013 and EN 15051-3: 2013 respectively.

The dustiness equivalent method (DEM) is based on single drop-down powder dispersion (0.5 g – 1.5 g powder sample mass per measurement) within a commercial fall shaft disperser (MEGAGRADIS, Sympatec GmbH, Clausthal-Zellerfeld, Germany) and subsequent size analysis by laser diffraction spectrometry (HELOS/KR-H2487, Sympatec GmbH, Clausthal-Zellerfeld, Germany) according to ISO 13320:2009. The intrinsically measured volume-weighted size distributions (based on Fraunhofer theory) over the diffraction equivalent diameter (corresponds to the projection area equivalent diameter) are used for computing dustiness equivalents. Therefore, the projection area equivalent diameter x_{geo} is at first converted into the aerodynamic diameter x_{ad} by assuming that the effective particle density equals the tapping density (c.f. (Barthel et al. 1998)):

$$x_{ad} = \sqrt{\frac{\rho_{eff}}{\rho_{ad}} \cdot x_{geo}^2}$$

To calculate dustiness data (i.e., for the inhalable, thoracic and alveolar dust fraction) equivalent to the CCD dustiness method of EN 15051, the volume-weighted size distributions over the aerodynamic equivalent diameter are afterwards combined with the separation functions for health relevant fractions according to EN 481:1993 up to a cut-off diameter of 37 µm (i.e., the technical cut-off diameter of the CDD method). Finally, the resulting quantities are expressed in the metric proposed by ECHA (i.e., in mg/kg metric).

Benchmark materials are defined independently for fibers and for particles:

FLU: OECD test material NM400/NM401 and commercial TCI C2154. NM400 has a low tendency to dust (150/mg/h) while TCI2154 is heavily dusting (8000/mg/h).

SRD: BaSO4_b (high dustiness) respirable mass-based: 1039±107 mg/kg; number-based 84.000±6.200/mg, was used by the CEN standardization project dustinano.

2.4.2 Sanding-induced particle release

To classify release data of different test methods for moderate mechanical stress situations, a comprehensive release testing program was performed on the base of three different setups for the simulation of sanding procedures. Detailed information on the setups and instruments operated by BASF (Neubauer, Wohlleben, and Tomović 2017), IUTA (Kuhlbusch and Kaminski 2014) and TUD (Gohler et al. 2013; Gohler et al. 2010)(ISO/DIS 21683:2018) can be gathered from the literature. For the purpose of release testing, the following conditions for sanding were applied:

Table SI_1 Comparison of conditions for sanding process simulation by BASF, IUTA and TUD for particle release characterisation.

setup	**SAN-BASF**	**SAN-IUTA**	**SAN-TUD**
kind of procedure	disc type sanding	disc type sanding	peripheral longitudinal sanding
mean cutting velocity	2.0 m/s	1.8 m/s	1.8 m/s
cutting power	N/A	N/A	1.3 W
paper graining	P400	P80 (P320 for coatings)	P600
analyses per sample	6	≥ 3	6 - 8
metric	fractional particle number concentration	fractional particle number concentration	fractional area-specific release numbers

Due to the different experimental design and metrics of the methods, received release data are not directly comparable. Assuming that a linear relationship holds true, the release data of each experimental setup (R_i) were scaled by release data gathered by each setup for the benchmark material epoxy.

$$\frac{R_{i,material}}{R_{i,benchmark}} = \frac{R_{SAN-BASF}}{7.1{\cdot}10^{5}\,\mathrm{cm^{-3}}} = \frac{R_{SAN-IUTA}}{2.4{\cdot}10^{3}\,\mathrm{cm^{-3}}} = \frac{R_{SAN-TUD}}{2.2{\cdot}10^{6}\,\mathrm{cm^{-2}}}$$

Figure SI_4 summaries the thus received scaled relative release quantities for each composite.

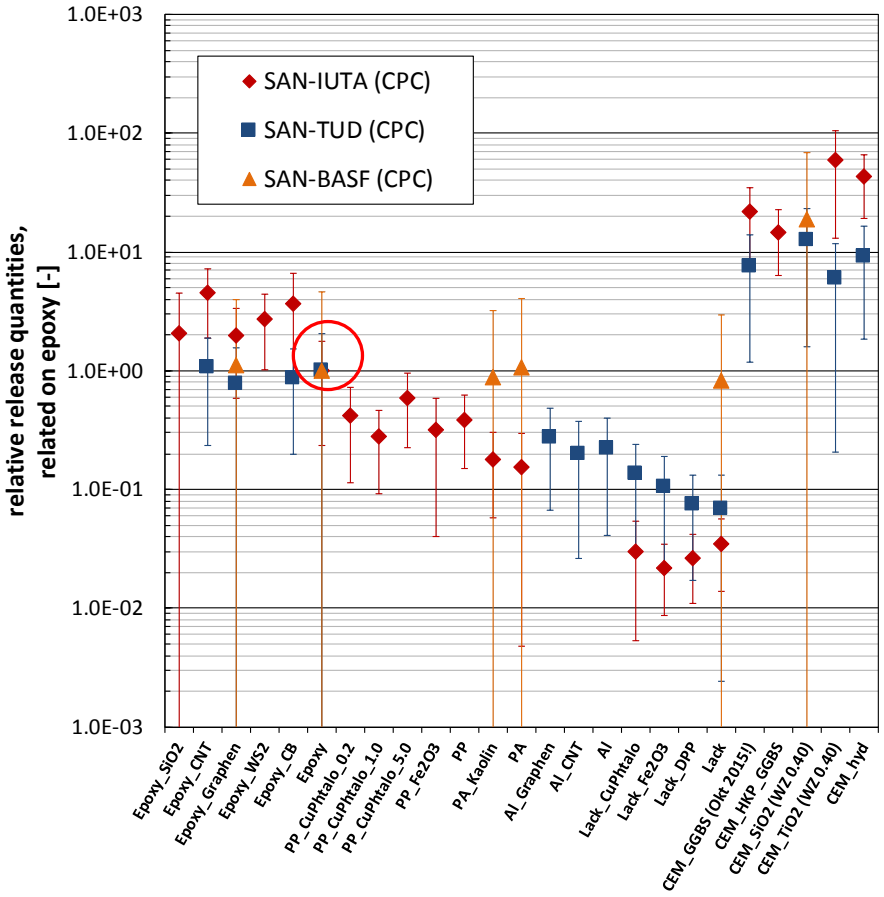

Figure SI_4 Relative sanding-induced particle release quantities (scaled by release quantities for epoxy) received by three different experimental methods; release data based on condensation particle counting (CPC), error bars are intensified due to simple error propagation calculation for non-correlated errors.

According to Figure SI_4 the scaled relative release quantities of the different setups correlate well among each other and establish a consistent ranking of release quantity via the matrix material:

$$R_{Lack,i} < R_{PA,i} < R_{PP,i} < R_{AL,i} < R_{Epoxy,i} < R_{CEM,i}$$

The experimental finding that the ranking is given by the matrix material, not be the embedded NF, is strong support of the grouping by matrix.

2.4.3 Agglomeration of the ENM upon NEP application

The methodology is not yet so mature that band boundaries could be derived. Projection analysis of particles on SEM / TEM images of bulk samples. The projected area A_{proj} of particles is determined using image analysis software (e.g. GIMP), which converts a number of pixels within the manually drawn outline of the particle into an area. For fibers we determine the projected area from the product of length and diameter. In each case, the total projected areas of the agglomerates A_a and the individual fibers A_p are determined.

2.4.3.1 Descriptors

The volume-based degree of agglomeration X_V is the quotient of the total volume of the agglomerates V_a and the sum of V_a and the accumulated volume of the primary particles V_{pp}:

$$X_V = \frac{V_a}{V_a + V_p} = \frac{d_a A_a}{d_a A_a + d_p A_p}.$$

The factors d_a and d_p are the diameters of the spheres with equivalent surface A_a and A_p.

2.4.3.2 Benchmark materials

GBS: BaSO4_b

Fibers: ARIGM001 ($X_V = 0.003$), NTX-3 ($X_V = 0.913$)

2.4.3.3 Band boundaries

Particles: A concrete band boundary is still being discussed.

For fibers analysed by the shaker method:

< 0.04	(low)
0.04 - 0.4	(medium)
> 0.4	(high)

Note: A high degree of agglomeration is considered beneficial in terms of risk potential.

2.4.4 Resilience of the NEP matrix

2.4.4.1 Method

Tensile elongation according to ISO 527 (for plastics)

2.4.4.2 Descriptors

Elongation at break or tensile strength

2.4.4.3 Benchmark materials

- Epoxy resin and cement
  - brittle
  - leads to exposed nanomaterials on the surface of fragments.
- Polyamide PA
  - soft / tough
  - leads to relatively coarser fragments with little or no exposed nanomaterials

2.4.4.4 Band boundaries

Elongation at break: 10% (Hirth et al. 2013)

Tensile strength: suitable for read-across, but no band boundary has been derived for grouping. (Schlagenhauf et al. 2015)

Both criteria are basically compatible with each other. In direct comparison of similar materials the tensile strength is more meaningful. (Neubauer, Wohlleben, and Tomović 2017)

2.4.5 Critical shapes upon release

2.4.5.1 Methods

Electron microscopy – Scanning and electron microscopy (SEM/TEM) is used to morphologically characterize particles collected on air samples. Discovered fibrous objects are measured.

2.4.5.2 Descriptors

Critical dimensions are (extended WHO criteria):

aspect ratio	>5:1	(as proposed by the ECHA guidance on nanoform registration)(ECHA 2017)
length	L >5µm	
diameter	20nm >d <3µm	

2.4.5.3 Benchmark materials

Currently, there is no commonly available MWCNT material (e.g. OECD NM series), which has shown a 0% WHO share in the Shaker procedure. Currently, we propose the material ARIGM002 as a benchmark material for the lower band boundary.

NM400 – MWCNT WHO share 0.4 %

NM401 – MWCNT WHO share 20.4%

2.4.5.4 Band boundaries

- Workplace: From the number of particles found with critical dimensions, the average concentration can be extrapolated during the sampling time, given known sampling conditions and filter area. Workstation band boundary is concentration <10,000 critical fibers (F) per m^3 (low), 10,000 F/m^3 to 100,000 F/m^3 (medium) and >100.00 F/m^3 (high).
- For laboratory tests (shaker method), the following band boundaries are discussed: percentages of the WHO objects to the total number of objects with the following limits: 0% (low), >0% to 1% (medium), and >1% (high)

2.5 Properties which describe „where they go: in relevant media“

2.5.1 Ion-releasing

In the grouping project of the UBA (FKZ: 3714 67 417 0) a methodology was proposed which is very compatible with the OECD draft TG dissolution (see above for solubility in water), and whose limit value lies at the detection limit of ion analysis (ICP-OES). (Hund-Rinke et al. 2018) With the expected advances in analytics, this is a temporally moving grouping. Instead, it is proposed here to apply exactly the same methodology through ultrafiltration after 24 hours, but to use the relevant (possibly more complex) medium. As a limit, 0.1 mg/L of ions at 100 mg/L particle concentration is proposed because this corresponds to the current Limit of Detection (LOD) of a multi-purpose elemental analysis.

2.5.2 Dissolution in relevant media

In nanoGRAVUR, an already known method for dissolution under non-equilibrium conditions was adapted to nanomaterials.(Koltermann-Jülly et al. 2018) Choice of medium depending on exposure scenario, in particular validated for inhalation with pH 4.5 with 2 mL/h, 1 mg nanomaterial in flow ultrafiltration cells, ion detection by ICP-MS + remaining-solids TEM after 7 days. The duration of 7 days is pragmatically fixed, and the limit was derived from the point of view of human toxicology. For ecotoxicology so far no statement can be made (results are evaluated, and OECD task force has been initiated in 2019). Benchmark materials for human inhalation can be derived:

- Non-persistent and high dissolution k>100 ng/cm²/h (ZnO NM110)
- Non-persistent, significant transformation k=1-100 ng/cm²/h ($BaSO_4$ NM220)
- Low dissolution, significant transformation k<1 ng/cm²/h (SiO_2 NM203)
- Low dissolution, low transformation k<1 ng/cm²/h (CeO_2 NM212)

2.5.3 Transformation „change of what they are “

The solids remaining after a dissolution test can also be analyzed. For this purpose, a preparation protocol was developed in nanoGRAVUR, which separates the salts and organics of the relevant medium (otherwise they become particles as drying artefacts), and the particles potentially transformed in their physical structure and / or chemical composition (= changed in "what they are "). Particles are prepared on a grid for TEM and image analysis to describe their size distribution, or by X-ray-Photoelectron Spectroscopy (XPS) with line shift analysis or Selected Area Diffraction (SAD) to

identify the chemical composition or crystal modification. An SOP is publicly available from nanoGRAVUR.

Metric: TEM + NanoDefiner Image evaluation: size distribution (D50 and polydispersity), average aspect ratio.

Benchmark materials for acidic pH 4.5: ZnO NM110 (particles disappear), $BaSO_4$ NM220 (Ostwald ripening: particles grow), CeO_2 NM212 (slight change).

Benchmark materials for neutral ADaM: $BaSO_4$ NM220 (Ostwald ripening: particles grow, become more crystalline).

2.5.4 Homo-agglomeration

In order to investigate the homo-agglomeration of NM in the relevant media, the following analyses are carried out in accordance with the newly established OECD TG318. Depending on the case study considered, the media can be varied, in this case DI water, medium with 5 mg/L Suwannee River humic acid + 0.01M $CaCl_2$ solution and a medium with 0.5 mg/L Suwannee River humic acid + 0.1 M $CaCl_2$ solution.

The selected nanomaterials are first dispersed according to the nanoGRAVUR SOP. Subsequently, the nanomaterials are added to the different media (target concentration 100 mg/L, if this does not leave the range specified by the TG318 range of agglomerates number of 10^{12}/L - this can be verified by the TG318 Annex (Excel) via the DLS data) (Abdolahpur Monikh et al. 2018) Subsequently, a) the hydrodynamic diameter (D50 in nm) is determined by DLS at different times (direct, 2h, 6h, 24h) and b) at the same times the supernatant of the samples will be taken and the concentration of nanomaterials in the supernatant will be determined by ICP-MS. For organic ENM the UV/Vis detection (TG318) can be used. This allows statements about agglomeration and sedimentation.

Band boundaries

In this case, nanomaterials which show more than 90% of the original concentration in the supernatant after 6 h are considered to be stable; the range between 10-90% is regarded as medium and materials <10% as unstable. Which limit values and whether the change in the hydrodynamic diameter (D50 value in nm) is used as a relevant parameter at the times mentioned is still under discussion, since with increasing agglomeration and sedimentation the uncertainty of the measurements by means of DLS increases in the supernatant.

Benchmark materials

There are currently no benchmark materials defined.

With the media of the TG318 Ag NM300 is "stable", whereas TiO_2 NM105 is "intermediate". The semi-soluble Ag material should be replaced in the medium term by a less soluble material, perhaps by colloidal silica such as SiO2_untreated.

2.5.5 Affinity (hetero-agglomeration)

Since it is known that in the environment the concentration of naturally occurring particles far exceeds the concentration of the ENM, it has been suggested in the literature that transport processes are much more determined by hetero-agglomeration than homo-agglomeration. The affinity of ENM to other particles would therefore be crucial (Geitner et al. 2016; Hendren et al. 2015) No methods were developed or tested in nanoGRAVUR, but we suspect that in the future parameters such as affinity α will also be relevant for groupings (Geitner et al. 2017; Geitner et al. 2016) An alternative method could also capture the affinity microscopically, with qualitative evaluation relative to a benchmark material.

In the current nanoGRAVUR scheme, the affinity is not used.

2.5.6 Mobility - soil

Method

To investigate the influence on mobility in soil compartments, soil column experiments based on the OECD TG312 in unsaturated soils are carried out. The changes to the OECD TG are pointed out in an SOP.

The experiments are carried out with a reference soil Refesol 01A

Descriptors

The concentration of nanomaterials in individual soil layers as well as in the eluate (measurement after 2h, 4h, 24h, 48h) is determined by ICP-MS.

Based on the data, mobility profiles are created in the soil columns.

In addition, before the experiments, the agglomeration and the zeta potential of the nanomaterials in aqueous suspension will be determined.

Band boundaries

At the moment it is not possible to get beyond a qualitative statement. Whether the results can be used for a read-across has yet to be clarified. How the results of the zeta potential and agglomeration can be transferred to the soil ecosystem has not yet been conclusively clarified.

Benchmark materials

There are currently no benchmark materials defined.

2.5.7 Mobility – systemic availability

Systemic availability is not a material property, but rather an in vivo toxicological finding. The homo-agglomeration in serum-containing medium was used as an extrinsic material property that correlated well with in vivo findings (one false positive, no false negatives) in the case studies of Arts et al..(Arts et al. 2016) This descriptor was also acquired in the context of nanoGRAVUR, and there was no contradiction to the in vivo findings. However, as nanoGRAVUR has not tested any systemically available particles, such as quantum dots of certain surface modifications,(Choi et al. 2010) no methodology can be conclusively recommended.

2.6 Properties which describe „what they do“

2.6.1 Reactiviy, abiotic

Methods were reviewed recently.(Hellack et al. 2017):

ESR: The reactivity of the nanomaterials is determined by the ability to form reactive oxygen species (ROS), often referred to as oxidative potential (OP). For measurements with ESR, two complementary approaches are used to detect different ROS species and a more general reactivity of NMs. For the first approach, the spin trap 5,5-dimethyl-1-pyrroline-N-oxide (DMPO) is used to detect the NM induced hydroxyl radical formation (OH•) in the presence of hydrogen peroxide (H_2O_2). Thus, in particular, the metallic NM-induced ROS formation is quantified by Fenton-like reactions. For the second approach, the spin probe 1-hydroxy-3-carboxy-pyrrolidine (CPH) is used, with which predominantly superoxide radicals (O_2•) and / or possible electron transfers are detected. Briefly, 100 µl of NM suspension was mixed with 100 µl CPH (1 mM in DFO-containing PBS) and incubated for 10 min at 37 °C before analysis by EPR spectroscopy.(Hellack, Nickel, and Schins 2017; Hellack et al. 2014)

The Analysis was done by ESR 300 Spectrometer MiniScope (Magnettech, Berlin, Germany) at room temperature. The CPH, and the DMPO were obtained from Alexis (Switzerland). The precision and

accuracy of the radical detection was based on repeated measurements and detection of internal standard CuSO4 solution (2.5 µM) and NM300 suspension (5 w/w%) (coefficient of variation, CV < 10 %) (Hellack, Nickel, and Schins 2017; Shi et al. 2003). Following EPR settings were used: magnetic field: 3365 G, sweep width: 100 G, scan time: 30 s, number of scans: 3, modulation amplitude: 1.975 G, receiver gain: 1000.

FRAS

The principle of the Ferric Reduction Ability of Serum (FRAS) assay is well established to assess oxidative damage, including its application to particle surface reactivity (Rogers et al. 2008). This assay has shown potential to separate active from passive NMs,(Pal et al. 2014; Hsieh et al. 2013), and to be specificially useful for grouping purposes.(Arts et al. 2016; Arts et al. 2015)

The assay was used in several nanosafety projects, especially the 137-material-comparison of Hsieh, Bello et al.(Hsieh et al. 2013) but by relatively few laboratories, and is not standardised yet (Hellack et al. 2017). An SOP including a dose-response-relationship was published in 2017 by nanoGRAVUR (Gandon et al. 2017) and is freely available http://iopscience.iop.org/1742-6596/838/1/012033 . In short, the antioxidative components present in human blood serum (HBS) serve as reporter molecules(Rogers et al. 2008) The assay separates the oxidative damage from the read-out of the reporter molecules, as schematically shown in Figure 1: (1), HBS is incubated with nanomaterials, which are then (2) removed by centrifugation. Afterwards (3) an aliquot of that pre-incubated HBS is mixed with a solution containing a Fe3+ complex and is again incubated. The ability of the pre-incubated HBS to reduce Fe3+ to Fe2+ is detected optically by a color change from transparent to blue. Any damage to anti-oxidative species in HBS by nanomaterials during step (1) will reduce the blue color in the final step (3). Within the nanoGRAVUR project, testing was performed in triplicate for both surface dose metrics and mass dose metrics. Based on the calibration of the antioxidant content of the serum against a known concentration of Trolox, a water soluble Vitamin E, the resulting units of oxidative damage are „Trolox-equivalent units (TEU)“ as nmol TEU per m² of dispersed ENM surface.(Pal et al. 2014; Hsieh et al. 2013)

Descriptors:

ESR: To determine the reactivity by means of ESR, both methods (DMPO and CPH) are used. For this, the spin trap + H_2O_2 or spin probe (without addition of H_2O_2) is added to a NM suspension (water or medium) and then the sample is measured. The results are related to blank.

FRAS: To improve sensitivity, two descriptors are extracted: the maximum biological oxidative damage in mass metric (mBOD)., and the maximum biological oxidative damage in surface metric (sBOD).

Whether a nanomaterial is rated as significantly reactive is assessed by FRAS relative to a negative benchmark, with the cutoffs: sBOD > 5 $nmol_{TEU}/m^2_{ENM}$; mBOD > 2 $nmol_{TEU}/mg_{ENM}$. ESR values are rated as significantly reactive in which the measured value is higher than the blank, including three times the standard deviation of the measurement, specifically values > 1.3 (i.e. 30% above the blank). For ESR, values larger than the reactivity of a reference material, e.g. Mn_2O_3 are considered "very reactive". For FRAS, the dynamic range is wider, and already values above 10% of the positive controls are scored as “very reactive”.

Band boundaries, human toxicity:

The results of the ESR and FRAS measurements are combined in a scoring system. In this case, 1/3 point is given for each “reactive” descriptor, and 1 point for each “very reactive” descriptor. A NM thus can get a maximum of 4 points (1 EPR mDMPO + 1 EPR mCPH + 1 FRAS sBOD + 1 FRAS mBOD). The mixed metric was a pragmatic choice of measurable descriptors that differentiate well between NFs. The aggregated score is rounded to integer values for Table 4. The resulting bands are: 1: low, 2: mid-low, 3: mid-high, 4: high.

However, specifically for grouping purposes, it is contemplated to use a uniform surface dose of 1 m^2/mL, giving a maximum of 3 points (1 sDMPO + 1 sCPH + 1 FRAS sBOD), but was not used here.

In future, one may thus perform a single-surface-dose variant of the ESR and FRAS assays (with a uniform surface dose, e.g. 1m²/L).

Band boundaries, ecotoxicity

The application of reactivity as a criterion of ecotoxicity grouping (across all (nano)materials) is viewed skeptically. The toxicity of the released ions seems to be much more important.

Benchmark materials

$BaSO_4$ (neg), Mn_2O_3 (pos) FRAS and $CuSO_4$ (pos) ESR are proposed as benchmark materials.

2.6.2 Reactivity, in vitro

The value of in vitro testing for a grouping of human inhalation toxicity has been described several times, (Arts et al. 2016), in particular with the nanoGRAVUR case studies. (Wiemann et al. 2016) Therefore, the nanoGRAVUR scheme also features the NR8383 macrophage assay with the well-known assessment scheme.(Wiemann et al. 2016). In vitro testing with NR8383 rat macrophages and the mode of evaluation were described in detail (Wiemann et al. 2016). In brief, cells were cultured under standard conditions (37 °C; 5 % CO_2) in F-12K medium supplemented with 2 mM glutamine, penicillin/streptomycin (100 U/10 mg/mL; and 15 % (v/v) fetal calf serum (FCS). For measuring the particle-induced release of lactate dehydrogenase activity (LDH), glucuronidase activity (GLU), tumour necrosis factor α (TNF) and hydrogen peroxide (H_2O_2) into the medium, cells were detached mechanically, seeded into 96-well plates ($3x10^5$ cells per well) and incubated in F-12K medium supplemented with 5 % FCS for 24 h. Cells were then incubated in F-12K medium (serum-free) with the particles for 16 h (LDH, GLU, and TNF-α), or in KRPG buffer for 1.5 h (H_2O_2). LDH was measured with a cytotoxicity kit (Roche, Germany) and GLU activity was measured with p-nitrophenyl-d-glucuronide (Sigma Aldrich, Germany). Both, LDH and GLU, were normalized to the lysate from Triton X-100 lysed cells (100% value). TNF was measured with a specific ELISA (bio-techne, Wiesbaden, Germany). H_2O_2 was quantified with the Amplex red assay (Sigma-Aldrich, Germany), using the formation of resorufin.
Statistical analysis: Macrophage data were generated in triplicates; three independent repetitions were carried out. Data were expressed as mean ± standard deviation (SD) and analyzed with Graph Pad Prism software (Version 6; GraphPad Software Inc., USA). To test for significance, test values were compared to those from non-treated vehicle controls using 2-way ANOVA and Dunnett's post hoc multiple comparison test. Test results with $p \leq 0.05$ were assessed as significant (*).

3 Bibliography of references in supporting information:

Abdolahpur Monikh, Fazel, Antonia Praetorius, Andrea Schmid, Philipp Kozin, Boris Meisterjahn, Ekaterina Makarova, Thilo Hofmann, and Frank von der Kammer. 2018. 'Scientific rationale for the development of an OECD test guideline on engineered nanomaterial stability', *NanoImpact*, 11: 42-50.

Amorim, Mónica J. B., Sijie Lin, Karsten Schlich, José M. Navas, Andrea Brunelli, Nicole Neubauer, Klaus Vilsmeier, Anna L. Costa, Andreas Gondikas, Tian Xia, Liliana Galbis, Elena Badetti, Antonio Marcomini, Danail Hristozov, Frank von der Kammer, Kerstin Hund-Rinke, Janeck J. Scott-Fordsmand, André Nel, and Wendel Wohlleben. 2018. 'Environmental Impacts by Fragments Released from Nanoenabled Products: A Multiassay, Multimaterial Exploration by the SUN Approach', *Environmental Science & Technology*.

Arts, Josje H. E., Mackenzie Hadi, Muhammad-Adeel Irfan, Athena M. Keene, Reinhard Kreiling, Delina Lyon, Monika Maier, Karin Michel, Thomas Petry, Ursula G. Sauer, David Warheit,

Karin Wiench, Wendel Wohlleben, and Robert Landsiedel. 2015. 'A decision-making framework for the grouping and testing of nanomaterials (DF4nanoGrouping)', *Regulatory Toxicology and Pharmacology*.

Arts, Josje H. E., Muhammad-Adeel Irfan, Athena M. Keene, Reinhard Kreiling, Delina Lyon, Monika Maier, Karin Michel, Nicole Neubauer, Thomas Petry, Ursula G. Sauer, David Warheit, Karin Wiench, Wendel Wohlleben, and Robert Landsiedel. 2016. 'Case studies putting the decision-making framework for the grouping and testing of nanomaterials (DF4nanoGrouping) into practice', *Regulatory Toxicology and Pharmacology*, 76: 234-61.

Babick, Frank, Johannes Mielke, Wendel Wohlleben, Stefan Weigel, and Vasile-Dan Hodoroaba. 2016. 'How reliably can a material be classified as a nanomaterial? Available particle-sizing techniques at work', *Journal of Nanoparticle Research*, 18: 1-40.

Barthel, Herbert, Mario Heinemann, Michael Stintz, and Benno Wessely. 1998. 'Particle Sizes of Fumed Silica', *Chemical Engineering & Technology*, 21: 745-52.

Choi, Hak Soo, Yoshitomo Ashitate, Jeong Heon Lee, Soon Hee Kim, Aya Matsui, Numpon Insin, Moungi G. Bawendi, Manuela Semmler-Behnke, John V. Frangioni, and Akira Tsuda. 2010. 'Rapid translocation of nanoparticles from the lung airspaces to the body', *Nat Biotech*, 28: 1300-03.

De Jong, Wim H., Eveline De Rijk, Alessandro Bonetto, Wendel Wohlleben, Vicki Stone, Andrea Brunelli, Elena Badetti, Antonio Marcomini, Ilse Gosens, and Flemming R. Cassee. 2018. 'Toxicity of copper oxide and basic copper carbonate nanoparticles after short-term oral exposure in rats', *Nanotoxicology*: 1-23.

ECHA. 2017. 'How to prepare registration dossiers that cover nanoforms: best practices'.

Farcal, Lucian, Fernando Torres Andón, Luisana Di Cristo, Bianca Maria Rotoli, Ovidio Bussolati, Enrico Bergamaschi, Agnieszka Mech, Nanna B. Hartmann, Kirsten Rasmussen, Juan Riego-Sintes, Jessica Ponti, Agnieszka Kinsner-Ovaskainen, François Rossi, Agnes Oomen, Peter Bos, Rui Chen, Ru Bai, Chunying Chen, Louise Rocks, Norma Fulton, Bryony Ross, Gary Hutchison, Lang Tran, Sarah Mues, Rainer Ossig, Jürgen Schnekenburger, Luisa Campagnolo, Lucia Vecchione, Antonio Pietroiusti, and Bengt Fadeel. 2015. 'Comprehensive In Vitro Toxicity Testing of a Panel of Representative Oxide Nanomaterials: First Steps towards an Intelligent Testing Strategy', *PLOS ONE*, 10: e0127174.

Funk, Birgit, Daniel Goehler, Bernhard Sachsenhauser, L Hillemann, M Stintz, S. Burkhard, Blake A Johnson, and Wendel Wohlleben. 2019. 'Impact of freeze-thaw weathering on integrity, internal structure and particle release from micro- and nanostructured cement composites', *submitted*.

Gandon, Arnaud, Kai Werle, Nicole Neubauer, and Wendel Wohlleben. 2017. "Surface reactivity measurements as required for grouping and read-across: An advanced FRAS protocol." In *Journal of Physics: Conference Series*, 012033. IOP Publishing.

Geitner, Nicholas K., Niall J. O'Brien, Amalia A. Turner, Enda J. Cummins, and Mark R. Wiesner. 2017. 'Measuring Nanoparticle Attachment Efficiency in Complex Systems', *Environmental Science & Technology*, 51: 13288-94.

Geitner, Nicholas, Stella Marinakos, Charles Guo, Niall O'Brien, and Mark Wiesner. 2016. 'Nanoparticle Surface Affinity as a Predictor of Trophic Transfer', *Environmental Science & Technology*, 50: 6663.

Gohler, D, A Nogowski, P Fiala, and M Stintz. 2013. 'Nanoparticle release form nanocomposites due to mechanical treatment at two stages of the life-cycle', *J Phys: Conf Ser*, 429: 012045.

Gohler, D, M Stintz, L Hillemann, and M Vorbau. 2010. 'Characterization of nanoparticle release from surface coatings by the simulation of a sanding process', *Ann Occup Hyg*, 54: 615 - 24.

Göhler, Daniel, and Michael Stintz. 2015. "Nanoparticle release quantification during weak and intense dry dispersion of nanostructured powders." In *Journal of Physics: Conference Series*, 012029. IOP Publishing.

Gosens, Ilse, Flemming R. Cassee, Michela Zanella, Laura Manodori, Andrea Brunelli, Anna Luisa Costa, Bas G. H. Bokkers, Wim H. de Jong, David Brown, Danail Hristozov, and Vicki Stone. 2016. 'Organ burden and pulmonary toxicity of nano-sized copper (II) oxide particles after short-term inhalation exposure', *Nanotoxicology*, 10: 1084-95.

Hamelmann, Frank, and Eberhard Schmidt. 2003. 'Methods of estimating the dustiness of industrial powders–a review', *KONA Powder and Particle Journal*, 21: 7-18.

Hellack, Bryan, Carmen Nickel, Catrin Albrecht, Thomas A. J. Kuhlbusch, Sonja Boland, Armelle Baeza-Squiban, Wendel Wohlleben, and Roel P. F. Schins. 2017. 'Analytical methods to assess the oxidative potential of nanoparticles: a review', *Environmental Science: Nano*, 4: 1920-34.

Hellack, Bryan, Carmen Nickel, and Roel P. F. Schins. 2017. 'Oxidative potential of silver nanoparticles measured by electron paramagnetic resonance spectroscopy', *Journal of Nanoparticle Research*, 19.

Hellack, Bryan, Aileen Yang, Flemming R. Cassee, Nicole A. H. Janssen, Roel P. F. Schins, and Thomas A. J. Kuhlbusch. 2014. 'Intrinsic hydroxyl radical generation measurements directly from sampled filters as a metric for the oxidative potential of ambient particulate matter', *Journal of Aerosol Science*, 72: 47-55.

Hendren, Christine Ogilvie, Gregory V. Lowry, Jason M. Unrine, and Mark R. Wiesner. 2015. 'A functional assay-based strategy for nanomaterial risk forecasting', *Science of The Total Environment*, 536: 1029-37.

Hirth, S., Lorenzo G. Cena, G. Cox, Z. Tomovic, Thomas M. Peters, and W. Wohlleben. 2013. 'Scenarios and methods that induce protruding or released CNTs after degradation of composite materials', *J.Nanoparticle Res.*, 15: 1504.

Hristozov, Danail, Lisa Pizzol, Gianpietro Basei, Alex Zabeo, Aiga Mackevica, Steffen Foss Hansen, Ilse Gosens, Flemming R. Cassee, Wim de Jong, Antti Joonas Koivisto, Nicole Neubauer, Araceli Sanchez Jimenez, Elena Semenzin, Vrishali Subramanian, Wouter Fransman, Keld Alstrup Jensen, Wendel Wohlleben, Vicki Stone, and Antonio Marcomini. 2018. 'Quantitative human health risk assessment along the lifecycle of nano-scale copper-based wood preservatives', *Nanotoxicology*: 1-19.

Hsieh, Shu-Feng, Dhimiter Bello, Daniel F. Schmidt, Anoop K. Pal, Aaron Stella, Jacqueline A. Isaacs, and Eugene J. Rogers. 2013. 'Mapping the Biological Oxidative Damage of Engineered Nanomaterials', *Small*, 9: 1853-65.

Hund-Rinke, Kerstin, Karsten Schlich, Dana Kühnel, Bryan Hellack, Heinz Kaminski, and Carmen Nickel. 2018. 'Grouping concept for metal and metal oxide nanomaterials with regard to their ecotoxicological effects on algae, daphnids and fish embryos', *NanoImpact*, 9: 52-60.

Keller, Jana, Wendel Wohlleben, Lan Ma-Hock, Volker Strauss, Sibylle Gröters, Karin Küttler, Karin Wiench, Christiane Herden, Günter Oberdörster, and Bennard van Ravenzwaay. 2014. 'Time course of lung retention and toxicity of inhaled particles: short-term exposure to nano-Ceria', *Archives of Toxicology*, 88: 2033-59.

Koltermann-Jülly, Johanna, Johannes G. Keller, Antje Vennemann, Kai Werle, Philipp Müller, Lan Ma-Hock, Robert Landsiedel, Martin Wiemann, and Wendel Wohlleben. 2018. 'Abiotic dissolution rates of 24 (nano)forms of 6 substances compared to macrophage-assisted dissolution and in vivo pulmonary clearance: Grouping by biodissolution and transformation', *NanoImpact*, 12: 29-41.

Kuhlbusch, Thomas, and Heinz Kaminski. 2014. 'Release from Composites by Mechanical and Thermal Treatment: Test Methods.' in, *Safety of Nanomaterials along Their Lifecycle: Release, Exposure, and Human Hazards* (Informa UK Limited).

Landsiedel, Robert, Lan Ma-Hock, Thomas Hofmann, Martin Wiemann, Volker Strauss, Silke Treumann, Wendel Wohlleben, Sibylle Gröters, Karin Wiench, and Bennard van Ravenzwaay. 2014. 'Application of short-term inhalation studies to assess the inhalation toxicity of nanomaterials', *Particle and Fibre Toxicology*, 11: 16.

Neubauer, Nicole, Lorette Scifo, Jana Navratilova, Andreas Gondikas, Aiga Mackevica, Daniel Borschneck, Perrine Chaurand, Vladimir Vidal, Jerome Rose, Frank von der Kammer, and Wendel Wohlleben. 2017. 'Nanoscale Coloristic Pigments: Upper Limits on Releases from Pigmented Plastic during Environmental Aging, In Food Contact, and by Leaching', *Environmental Science & Technology*, 51: 11669-80.

Neubauer, Nicole, Wendel Wohlleben, and Željko Tomović. 2017. 'Conductive plastics: comparing alternative nanotechnologies by performance and life cycle release probability', *Journal of Nanoparticle Research*, 19: 112.

Ogura, Isamu, Hiromu Sakurai, and Masashi Gamo. 2009. "Dustiness testing of engineered nanomaterials." In *Journal of Physics: Conference Series*, 012003. IOP Publishing.

Oomen, Agnes G., Klaus Günter Steinhäuser, Eric A. J. Bleeker, Fleur van Broekhuizen, Adriënne Sips, Susan Dekkers, Susan W. P. Wijnhoven, and Philip G. Sayre. 2018. 'Risk assessment frameworks for nanomaterials: Scope, link to regulations, applicability, and outline for future directions in view of needed increase in efficiency', *NanoImpact*, 9: 1-13.

Pal, AnoopK, Shu-Feng Hsieh, Madhu Khatri, JacquelineA Isaacs, Philip Demokritou, Peter Gaines, DanielF Schmidt, EugeneJ Rogers, and Dhimiter Bello. 2014. 'Screening for oxidative damage by engineered nanomaterials: a comparative evaluation of FRAS and DCFH', *Journal of Nanoparticle Research*, 16: 1-20.

Pang, Chengfang, Nicole Neubauer, Matthew Boyles, David Brown, Nilesh Kanase, Danail Hristozov, Teresa Fernandes, Vicki Stone, Wendel Wohlleben, and Antonio Marcomini. 2017. 'Releases

from transparent blue automobile coatings containing nanoscale copper phthalocyanine and their effects on J774 A1 macrophages', *NanoImpact*, 7: 75-83.

Pantano, Daniele, Nicole Neubauer, Jana Navratilova, Lorette Scifo, Chiara Civardi, Vicki Stone, Frank von der Kammer, Philipp Müller, Marcos Sanles Sobrido, Bernard Angeletti, Jerome Rose, and Wendel Wohlleben. 2018. 'Transformations of Nanoenabled Copper Formulations Govern Release, Antifungal Effectiveness, and Sustainability throughout the Wood Protection Lifecycle', *Environmental Science & Technology*.

Pizzol, Lisa, Danail Hristozov, Alex Zabeo, Gianpietro Basei, Wendel Wohlleben, Antti Joonas Koivisto, Keld Alstrup Jensen, Wouter Fransman, Vicki Stone, and Antonio Marcomini. 2019. 'SUNDS probabilistic human health risk assessment methodology and its application to organic pigment used in the automotive industry', *NanoImpact*, 13: 26-36.

Plitzko, S, E Gierke, N Dziurowitz, and D Broßell. 2010. 'Erzeugung von CNT/CNF-Stäuben mit einem Schwingbett-Aerosolgenerator und Charakterisierung der Fasermorphologie mithilfe eines Thermalpräzipitators als Sammelsystem', *Gefahrstoffe-Reinhaltung der Luft*, 70: 31.

Rasmussen, K, J Mast, PJ De Temmerman, E Verleysen, N Waegeneers, F Van Steen, J Christophe Pizzolon, L De Temmerman, E Van Doren, and KA Jensen. 2014. 'Multi-walled carbon nanotubes, NM-400, N, M-401, NM-402, NM-403: characterisation and physico-chemical properties. JRC Repository: NM-series of Representative Manufactured Nanomaterials European Commission-Joint Research Centre', *Institute for Health and Consumer Protection. Available at: http://publications. jrc. ec. europa. eu/repository/handle/JRC91205*.

Retamal, M, F Babick, and M Stintz. 2017. 'Ultrasonic dispersion of nanostructured materials with probe sonication− practical aspects of sample preparation', *Powder Technology*, 318: 451-58.

Rogers, E. J., S. F. Hsieh, N. Organti, D. Schmidt, and D. Bello. 2008. 'A high throughput in vitro analytical approach to screen for oxidative stress potential exerted by nanomaterials using a biologically relevant matrix: Human blood serum', *Toxicology in Vitro*, 22: 1639-47.

Schlagenhauf, Lukas, Tina Buerki-Thurnherr, Yu-Ying Kuo, Adrian Wichser, Frank Nüesch, Peter Wick, and Jing Wang. 2015. 'Carbon Nanotubes Released from an Epoxy-Based Nanocomposite: Quantification and Particle Toxicity', *Environmental Science & Technology*, 49: 10616-23.

Schneider, S., R. Landsiedel, W. Wohlleben, A. Wolterbeek, I. Waalkens-Berendsen, and H. van de Sandt. 2011. 'Oral prenatal developmental toxicity study with NM-200 synthetic amorphous silica in Wistar rats', *Reproductive Toxicology*, 32: 173-74.

Schneider, T., and K. A. Jensen. 2008. 'Combined single drop and rotating drum dustiness test of fine to nanosized powders using a small drum', *Annals of Occupational Hygiene*, 52: 23-34.

Shi, T., R. P. Schins, A. M. Knaapen, T. Kuhlbusch, M. Pitz, J. Heinrich, and P. J. A. Borm. 2003. 'Hydroxyl radical generation by electron paramagnetic resonance as a new method to monitor ambient particulate matter composition', *Journal of Environmental Monitoring*, 5: 550-56.

Singh, C., S. Friedrichs, N. Gibson, K. A. Jensen, M. Levin, R. Birkedal, G. Pojana, W. Wohlleben, S. Schulte, K. Wiench, D. Marshall, K. Hund-Rinke, W. K”rdel, and C. L. Klein. 2011. "NM-Series of Representative Manufactured Nanomaterials: Zinc Oxide NM-110, NM-111, NM-112, NM-113. Characterisation and test item preparation." In.

Visic, B., L. S. Panchakarla, and R. Tenne. 2017. 'Inorganic Nanotubes and Fullerene-like Nanoparticles at the Crossroads between Solid-State Chemistry and Nanotechnology', *Journal of the American Chemical Society*, 139: 12865-78.

Wiemann, Martin, Antje Vennemann, Ursula G. Sauer, Karin Wiench, Lan Ma-Hock, and Robert Landsiedel. 2016. 'An in vitro alveolar macrophage assay for predicting the short-term inhalation toxicity of nanomaterials', *Journal of Nanobiotechnology*, 14: 1-27.

Wohlleben, Wendel, Marc D. Driessen, Simon Raesch, Ulrich F. Schaefer, Christine Schulze, Bernhard von Vacano, Antje Vennemann, Martin Wiemann, Christian A. Ruge, Herbert Platsch, Sarah Mues, Rainer Ossig, Janina M. Tomm, Jürgen Schnekenburger, Thomas A. J. Kuhlbusch, Andreas Luch, Claus-Michael Lehr, and Andrea Haase. 2016. 'Influence of agglomeration and specific lung lining lipid/protein interaction on short-term inhalation toxicity', *Nanotoxicology*: 1-11.

Zohar, Elad, Sharon Baruch, Mark Shneider, Hanna Dodiuk, Samuel Kenig, Reshef Tenne, and H. Daniel Wagner. 2011. 'The Effect of WS2 Nanotubes on the Properties of Epoxy-Based Nanocomposites', *Journal of Adhesion Science and Technology*, 25: 1603-17.

EN 481:1993. Workplace atmospheres - Size fractions for measurement of airborne particles

ISO 13320:2009. Particle size analysis - Laser diffraction methods

ISO/DIS 21683:2018. Pigments and extenders - Determination of experimentally simulated nano-object release from paints, varnishes and pigmented plastics.